

Chaotic microcavity laser with high quality factor and unidirectional output

Qinghai Song,¹ Wei Fang,² Boyang Liu,³ Seng-Tiong Ho,³ Glenn S. Solomon,² and Hui Cao^{1,*}

¹*Department of Applied Physics, Yale University, New Haven, Connecticut 06520-8482, USA*

²*Joint Quantum Institute, NIST and University of Maryland, Gaithersburg, Maryland 20899, USA*

³*Department of Electrical Engineering and Computing Science, Northwestern University, Evanston, Illinois 60208, USA*

(Received 31 May 2009; published 20 October 2009)

We demonstrate a chaotic microcavity laser whose quality is comparable to typical nonchaotic microcavity lasers, yet it has the unique characteristic of unidirectional output. The cavity shape is a disk with the boundary defined by a curve called limaçon of Pascal. For a lasing mode of volume less than $0.2 \mu\text{m}^3$, the measured quality factor is 23 000. The record-high quality and small modal volume result in extremely low-lasing threshold. The spontaneous emission coupling efficiency is approximately 6% and is the reported value for a chaotic microcavity laser. All the lasing modes have one output beam in the same direction with a divergence angle less than 40° . This universal directionality is determined by the chaotic ray dynamics in the open cavity.

DOI: [10.1103/PhysRevA.80.041807](https://doi.org/10.1103/PhysRevA.80.041807)

PACS number(s): 42.55.Sa, 42.55.Px, 05.45.Mt, 42.60.Da

A semiconductor microdisk cavity achieves strong optical confinement by total internal reflection of light at disk boundary, which leads to the formation of whispering gallery (WG) modes [1,2]. These cavities can have high quality factor (Q) and low mode volume and have been used in a variety of experiments ranging from solid-state cavity quantum electrodynamics [6] to low-threshold lasing [3–5]. A limitation of the standard circular disk is the isotropic output emission. Deformation of cavity shape from cylindrical symmetry is straight forward way of obtaining directional output [7,8]; as is waveguide coupling even though it requires precise positioning of a waveguide next to or underneath the cavity [9–12]. However, deformed microcavities suffer Q spoiling, which results in high lasing thresholds, and most deformed microdisk lasers produce multiple output beams. For many experiments and applications, such as microlasers and single-photon sources, a single output beam is required. Cavity with unique shapes, such as spiral and rounded isosceles, have shown unidirectional emission [13–15]. The divergence angle of output beam from the spiral cavity is over 60° and that from the rounded isosceles about 80° . Their Q s are low; for instance, the Q of the rounded isosceles is only 40. A better type of deformed microcavity is the interior WG mode cavity, where the modes are located close to the cavity center. This cavity can have $Q \sim 6000$ and unidirectional output of divergence angle $30^\circ - 40^\circ$ [16,17]. However, the normal circumferential WG modes coexist. They have higher Q and reduce the overall unidirectionality. Furthermore, they dominate lasing in the case of uniform excitation and produce the normal nondirectional output. Carrier injection to the cavity center selects interior WG modes for lasing because they have better spatial overlap with the gain region. However, this selective pumping method is very difficult to implement in microcavities smaller than $5 \mu\text{m}$. Another proposed scheme for obtaining unidirectional emission from high- Q modes is to couple a low- Q mode with unidirectional output to a high- Q mode [18]. Unfortunately this approach works

only for particular modes and the existence of nearly degenerate modes with different far-field patterns smears out the output directionality.

A counterintuitive way of obtaining unidirectional output is to utilize a chaotic cavity [19]. The common expectation for modes of a chaotic dielectric cavity is low- Q factor and nearly random emission pattern [20]. This is because an optical ray undergoing chaotic diffusion in the angular momentum space can quickly reach the leaky region (where the incident angle χ at cavity boundary is less than the critical angle χ_c for total internal reflection) and escape from the cavity by refraction. However, unstable periodic orbits (UPOs) exist in the chaotic cavities and are manifested in the cavity resonances. In particular, some cavity modes exhibit increased field intensity near UPOs and are called scar modes. These scar modes can have high- Q factors if the UPOs are located outside the leaky region in the angular momentum space [21,22]. Their emissions are often directional as the rays starting near the UPOs diffuse to the leaky region along certain preferred routes defined by the unstable manifolds [20,23–26]. The chaotic microcavity lasers that have been fabricated so far have multidirectional output [27,28]. For example, for both semiconductor and polymer cavities with diameters of approximately $100 \mu\text{m}$, four beams result, each with a divergence angle of $10^\circ - 15^\circ$. Despite the large cavity size, the quality factor is ~ 6000 [29]. Recently Wiersig and Hentschel proposed a type of chaotic microcavity that produces unidirectional emission and has high quality [30]. The cavity boundary is defined by the limaçon of Pascal: $\rho = R(1 + \epsilon \cos \theta)$, where ρ and θ are the radial coordinate and polar angle respectively. Although the intracavity ray dynamics is predominantly chaotic, wave localization on the UPOs with $\chi > \chi_c$ leads to the formation of high- Q scar modes. The output directionality is universal for all the high- Q scar modes because the corresponding escape routes of rays are similar [30].

In this Rapid Communication we report lasing in the limaçon-shaped GaAs microdisks with embedded InAs quantum dots (QDs) as the gain medium. The measured Q factor is approximately 23 000 for a disk dimension is less than $5 \mu\text{m}$. The Q is significantly higher than all previously reported Q values for deformed microcavities [13,17], while

*Author to whom correspondence should be addressed; hui.cao@yale.edu

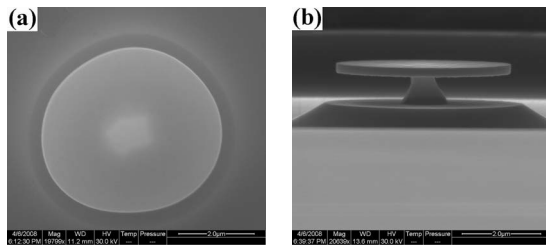


FIG. 1. Scanning electron microscope images of a GaAs microdisk on top of a $\text{Al}_{0.68}\text{Ga}_{0.32}\text{As}$ pedestal. (a) Top view and (b) tilt view. The pedestal is etched to have a top lateral dimension of 620 nm.

simultaneously having smaller mode volume. The high quality factor and small modal volume result in very low-lasing threshold, allowing continuous-wave operation. All the lasing modes have single output beam in the same direction, regardless of their wavelengths and intracavity mode structures. Our numerical simulations show two types of high- Q modes in the limaçon cavity: the previously mentioned scar modes [30] and a new type of mode for the limaçon cavity: whispering-gallery-like modes formed by dynamical localization. Unlike scar modes, these modes do not correspond to closed ray orbits; yet, they often have higher Q s than the scar modes and are responsible for the observed low-lasing thresholds.

The sample is epitaxially deposited on a GaAs substrate by molecular-beam epitaxy. The layer structure consists of 1000 nm $\text{Al}_{0.68}\text{Ga}_{0.32}\text{As}$ and 265 nm GaAs. Inside the GaAs layer there are six uncoupled layers of InAs QDs equally spaced by 25 nm GaAs barriers. The areal density of InAs QDs is $\sim 10^{11} \text{ cm}^{-2}$, and their inhomogeneous linewidth is about 50 nm. Limaçon-shaped microdisks are fabricated with photolithography and two steps of wet etching. The first step is a nonselective etching with HBr followed by a HF-based selective etching to undercut $\text{Al}_{0.68}\text{Ga}_{0.32}\text{As}$. Figure 1 shows the top-view and tilt-view scanning electron microscope (SEM) images of a GaAs microdisk. The disk boundary is a good fit to the limaçon curve with $\epsilon=0.45$ and $R=2.18 \mu\text{m}$.

In the lasing experiment, the sample is mounted in a liquid Helium cryostat. The substrate temperature is kept at 10 K. The microdisk is optically pumped by a CW diode laser (wavelength=775 nm) or a mode-locked Ti:Sapphire laser (pulse width=200 fs pulses, repetition rate=76 MHz repetition rate, center wavelength=790 nm). A long-working-distance (LWD) objective lens with a numerical aperture of 0.4 focuses the pump beam to a single disk from the top. A

small amount of emission from the microdisk is scattered by the disk boundary to the top and collected by the same objective lens. Another lens collects the in-plane emission from the disk side and direct it through a linear polarizer. The incident pump power was measured in front of the LWD objective lens by a power meter. The size of pump spot on the sample surface was measured by imaging it to a charge coupled device (CCD) camera. The pump intensity was then computed. Time-integrated emission spectra are taken by a 0.55 m spectrometer with a 1800 groove/mm grating and a liquid-nitrogen-cooled CCD array detector. The entrance slit is $20 \mu\text{m}$ and the spectral resolution is about 0.016 nm. Figure 2(a) is part of a time-integrated emission spectrum obtained with continuous-wave (CW) pumping. It consists of several narrow peaks. Figure 2(b) shows the intensity I and linewidth $\Delta\lambda$ of one peak at $\lambda=998 \text{ nm}$ as a function of the incident pump intensity P . The variation in $\log I$ with $\log P$ exhibits a S -shape with two kinks at $P \approx 102$ and 300 W/cm^2 . The first kink corresponds to the transition from linear increase in I with P to superlinear increase. Since the superlinear increase is caused by light amplification, the first kink represents the onset of optical gain, i.e., the transparency threshold. Above the second kink the increase in I with P becomes linear again due to gain saturation. The linewidth drops rapidly with increasing P , eventually approaching the resolution of our spectrometer ($\sim 0.016 \text{ nm}$). These data demonstrate lasing in the limaçon cavity. We estimate the Q factor from the linewidth at the transparency threshold. In Fig. 2(b) $\Delta\lambda \approx 0.046 \text{ nm}$ at the first kink of $\log I - \log P$ curve. The linewidth did not change when the entrance slit width of the spectrometer was reduced from $20 \mu\text{m}$ to $10 \mu\text{m}$, indicating the spectral resolution is limited by the CCD pixel size instead of the slit width. After deconvoluting the spectral resolution (0.016 nm) from the measured linewidth, we obtained the actual linewidth of 0.043 nm. Thus the quality factor of this mode is about 23 000. The spontaneous emission coupling efficiency β , which represents the percentage of spontaneously emitted photons to the lasing mode, is estimated from the threshold curve in Fig. 2(b) [31]. Its value is approximately 6%, comparable to typical nonchaotic microcavity lasers [32,33]. β is usually larger for a microcavity of smaller size and higher quality factor. Since all previously realized chaotic microcavity lasers have lower Q and larger modal volume than our limaçon cavity, their β values shall be smaller than ours. However, β has been measured for a chaotic microcavity.

To measure the far-field pattern of laser emission from a limaçon cavity, we fabricate a ring structure around each microdisk. The in-plane laser emission from the disk edge

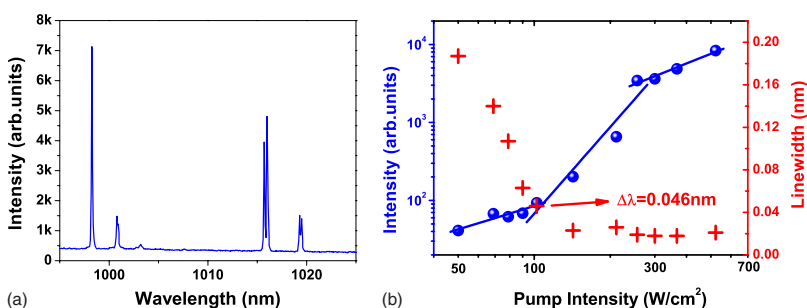


FIG. 2. (Color online) Experimental results of lasing in the limaçon microcavity under CW pumping. (a) Part of a time-integrated emission spectrum taken at the incident pump intensity $P=522 \text{ W/cm}^2$. (b) Intensity I (blue dots) and spectral width (red crosses) of one peak at $\lambda=998 \text{ nm}$ as a function of incident pump intensity P . The slope is equal to 0.99 below the first kink, 3.68 between the first and second kinks, and 1.01 above the second kink.

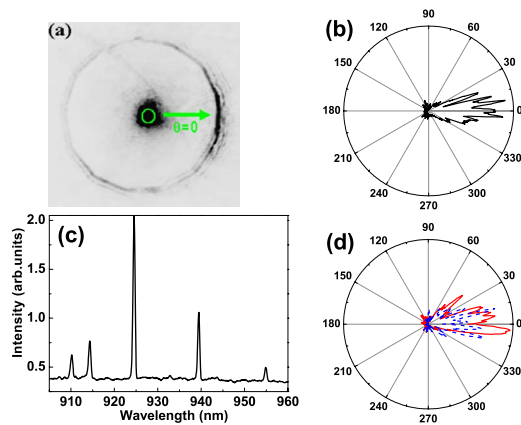


FIG. 3. (Color online) Measured directionality of laser emission from the limaçon microcavity pumped by Ti:Sapphire laser. The incident pump power is 92 W/cm^2 . (a) An image of laser emission from the microdisk scattered by the ring $34 \mu\text{m}$ away from the disk. (b) Far-field angular distributions of emission intensities of all lasing modes. (c) Time-integrated emission spectrum taken simultaneously with the far-field emission pattern. (d) Far-field angular distributions of two lasing modes at $\lambda=909 \text{ nm}$ (red line) and 923 nm (blue dashed line).

propagates to the ring and is scattered out of the plane. The scattered light pattern is imaged by the objective lens to a CCD camera. Since the ring radius exceeds $4R^2/\lambda$, the scattered light intensity along the ring reflects the far-field emission pattern of the microdisk. Figure 3(a) is an image of laser emission from microdisk scattered by the ring. It shows the laser output from the limaçon cavity is predominately in one direction. As shown in Fig. 3(b), the output beam is centered around $\theta=0$ with a width of 40° . We compute the fraction of far-field emission as a function of subtended angle. 68% of total emission intensity is confined within $|\theta| \leq 40^\circ$ and about 50% of emission within $|\theta| \leq 20^\circ$. The emission spectrum taken simultaneously with the image [Fig. 3(c)] reveals multimode lasing. Hence, the directional emission shown in Fig. 3(b) comes from all lasing modes. To obtain the far-field emission pattern of individual lasing modes, we place an interference filter in front of the CCD camera to select only one mode. The passband of the filter is $\sim 10 \text{ nm}$ wide in wavelength. By tilting the filter, we can tune the center wavelength of passband and image different lasing modes. Figure 3(d) shows the far-field patterns of two lasing modes at wavelength 909 and 923 nm. They are similar to that of total laser emission except for a small variation in angular distribution of output intensity. Therefore, all the lasing modes have output beams in the same direction with similar divergence angle.

To understand the lasing modes, we have performed numerical simulations of actual microdisks that are measured ($\epsilon=0.45$ and $R=2.18 \mu\text{m}$). The effective refractive index is set at 3.13. Our polarization measurement of in-plane emission from the disk side illustrates that all the lasing modes are transverse electric (TE) polarized (the electric field is parallel to the disk plane). Since the pump intensity is uniform across the disk, the lasing modes correspond to high- Q TE resonances, which we calculate by solving the Maxwell's

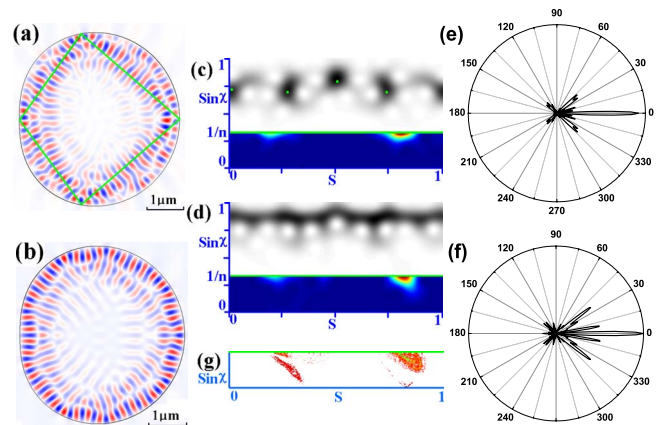


FIG. 4. (Color online) (a), (c), (e) and (b), (d), (f) are field pattern, Husimi projections, and far-field angular distributions of resonant modes at 945 and 928 nm, respectively. (g) is the distribution of optical ray amplitude in the leaky region obtained by classical ray tracing with 20 000 uniformly distributed rays.

equations numerically. However, we cannot obtain one-to-one correspondence between the observed lasing modes and the calculated high- Q modes due to uncertainty in determining the values of refractive index and its dispersion. The microdisk is separated from the substrate by a pedestal, and can be heated by the pump light. The exact temperature of microdisk, and thus the temperature-dependent refractive index, is not known. During pulse excitation, the refractive index changes in time because of rapid variation in carrier density. Without including these complications, our numerical calculations aim to illustrate the characteristic of lasing modes that usually correspond to high- Q modes.

Our simulation indicates there are two types of high- Q modes in the limaçon cavity: (i) the classic scar modes as predicted by Wiersig and Hentschel [30]; and (ii) different WG-like modes formed by dynamical localization. The spatial intensity distribution of a typical scar mode is shown in Fig. 4(a). Its wavelength $\lambda=945 \text{ nm}$, $Q=15\,000$, and modal volume $V_m=0.15 \mu\text{m}^3$. To identify the corresponding ray orbit, we calculate the intensity and incident angle of light along the cavity boundary [Fig. 4(c)]. This mode is localized on a UPO [drawn in Fig. 4(a)] with four bounces from the cavity boundary [marked as green dots in Fig. 4(c)]. The angular distribution of far-field intensity, plotted in Fig. 4(e), exhibits single output beam in the direction $\theta=0$.

The second type of high- Q modes do not correspond to closed orbits like the scar modes, yet they have higher quality factor than the scar modes. Thus they are more likely to be the lasing modes because of lower lasing threshold. Figure 4(b) shows a simulation of one such mode at $\lambda=928 \text{ nm}$. Its $Q=94\,000$ and $V_m=0.19 \mu\text{m}^3$. Figure 4(d) shows that the intensity is distributed approximately uniformly along the cavity boundary, and the incident angle χ of light at the boundary is nearly constant. Thus, it is similar to a WG mode even though the classic WG mode cannot exist in such a small limaçon cavity. By integrating the mode intensity in Fig. 4(d) over s , we obtain its distribution in $\sin \chi$. The integrated intensity decays exponentially away from the maximal value at $\sin \chi_0=0.84$. The localization length esti-

mated from the decay length is about 0.1. Since it is smaller than the distance (~ 0.52) from the mode center ($\sin \chi_0 = 0.84$) to the critical line ($\sin \chi_c = 0.32$), this mode is dynamically localized in the angular momentum $m = nkR \sin \chi$ [34,35]. Chaotic diffusion of rays toward lower χ is suppressed because of their destructive interference, leading to the formation of WG-like mode. The exponentially small modal intensity in the leaky region (where $\sin \chi < 1/n$, and n is the refractive index of microdisk) results in extraordinarily high- Q factor. In real space the field intensity is very low in the disk center, avoiding Q degradation by scattering of the pedestal below the center of the disk. Although its intracavity mode structure is quite different from that of a scar mode, the far-field pattern is similar. As shown in Fig. 4(f), the WG-like mode has emission predominantly in the direction θ near 0. The color-enhanced intensity distribution in the leaky region [Fig. 4(d)] illustrates that the escape route of light from the cavity for the WG-like mode is similar to that of the scar mode [Fig. 4(c)]. Our ray tracing calculation reveals the escape route of optical rays in Fig. 4(g). The distribution of ray amplitude in the leaky region resembles that of modal intensity, confirming the universal output directionality results from classical ray dynamics in the open cavity.

In conclusion, we have achieved simultaneously low-lasing threshold and unidirectional emission using a limaçon microcavity of dimension less than $5 \mu\text{m}$. The measured Q factor is about 23 000, much larger than that of all other deformed microcavities. It is comparable to the Q factor of most circular microdisks with similar size and also fabricated by photolithography and wet chemical etching [36]. The high quality and small modal volume lead to a spontaneous emission coupling efficiency of $\sim 6\%$, similar to that of typical nonchaotic microcavity laser. All the lasing modes in the limaçon cavity have output beams in the same direction. The divergence angle is about 40° , larger than the theoretical value due to cavity sidewall roughness. The output directionality as well as the cavity Q factor can be further improved by increasing the fabrication accuracy with e-beam lithography, optimized resist reflow and dry etching techniques [12].

We acknowledge Professor A. D. Stone for fruitful discussions and critical reading of this Rapid Communication. We also thank Professor J. Wiersig, Professor E. Bogomolny, and Dr. M. Hentschel for stimulating discussions. This work was supported partly by NIST under the Grant No. 70NANB6H6162 and by NSF under the Grant No. DMR-0808937.

-
- [1] R. K. Chang and A. J. Campillo, *Optical Processes in Microcavities* (World Scientific, Singapore, 1996).
- [2] K. J. Vahala, *Nature (London)* **424**, 839 (2003).
- [3] S. L. McCall *et al.*, *Appl. Phys. Lett.* **60**, 289 (1992).
- [4] C. P. Michael *et al.*, *Appl. Phys. Lett.* **90**, 051108 (2007).
- [5] T. J. Kippenberg, J. Kalkman, A. Polman, & K. J. Vahala, *Phys. Rev. A* **74**, 051802(R) (2006).
- [6] E. Peter *et al.*, *Phys. Rev. Lett.* **95**, 067401 (2005).
- [7] J. U. Nockel and A. D. Stone, *Nature (London)* **385**, 45 (1997).
- [8] C. Gmachl *et al.*, *Science* **280**, 1556 (1998).
- [9] J. P. Zhang *et al.*, *IEEE Photonics Technol. Lett.* **8**, 968 (1996).
- [10] T. J. Kippenberg, S. M. Spillane, D. K. Armani, and K. J. Vahala, *Appl. Phys. Lett.* **83**, 797 (2003).
- [11] S. J. Choi, K. Djordjev, S. J. Choi, and P. D. Dapkus, *IEEE Photonics Technol. Lett.* **15**, 1330 (2003).
- [12] K. Srinivasan and O. Painter, *Nature (London)* **450**, 862 (2007).
- [13] G. D. Chern *et al.*, *Appl. Phys. Lett.* **83**, 1710 (2003).
- [14] M. Kneissl *et al.*, *Appl. Phys. Lett.* **84**, 2485 (2004).
- [15] M. S. Kurdoglyan, S.-Y. Lee, S. Rim, and C.-M. Kim, *Opt. Lett.* **29**, 2758 (2004).
- [16] Y. Baryshnikov, P. Heider, W. Parz, and V. Zharnitsky, *Phys. Rev. Lett.* **93**, 133902 (2004).
- [17] J. Gao *et al.*, *Appl. Phys. Lett.* **91**, 181101 (2007).
- [18] J. Wiersig and M. Hentschel, *Phys. Rev. A* **73**, 031802(R) (2006).
- [19] A. D. Stone, *Phys. Scr.* **T90**, 248 (2001).
- [20] H. G. L. Schwefel *et al.*, *J. Opt. Soc. Am. B* **21**, 923 (2004).
- [21] W. Fang, A. Yamilov, and H. Cao, *Phys. Rev. A* **72**, 023815 (2005).
- [22] S. Y. Lee, M. S. Kurdoglyan, S. Rim, and C. M. Kim, *Phys. Rev. A* **70**, 023809 (2004).
- [23] S. Y. Lee *et al.*, *Phys. Rev. A* **72**, 061801(R) (2005).
- [24] S. Shinohara and T. Harayama, *Phys. Rev. E* **75**, 036216 (2007).
- [25] S. Shinohara, T. Harayama, H. E. Türeci, and A. D. Stone, *Phys. Rev. A* **74**, 033820 (2006).
- [26] Lee, S.-B. *et al.*, *Phys. Rev. A* **75**, 011802(R) (2007).
- [27] T. Harayama *et al.*, *Phys. Rev. E* **67**, 015207(R) (2003).
- [28] M. Lebental, J. S. Lauret, R. Hierle, and J. Zyss, *Appl. Phys. Lett.* **88**, 031108 (2006).
- [29] S. Shinohara, T. Fukushima, and T. Harayama, *Phys. Rev. A* **77**, 033807 (2008).
- [30] J. Wiersig and M. Hentschel, *Phys. Rev. Lett.* **100**, 033901 (2008).
- [31] G. Bjork, H. Heitmann, and Y. Yamamoto, *Phys. Rev. A* **47**, 4451 (1993).
- [32] K. Srinivasan, M. Borselli, O. Painter, A. Stintz, and S. Krishna, *Opt. Express* **14**, 1094 (2006).
- [33] H. Takashima, H. Fujiwara, S. Takeuchi, K. Sasaki, and M. Takahashi, *Appl. Phys. Lett.* **92**, 071115 (2008).
- [34] O. A. Starykh, P. R. J. bJacquod, E. E. Narimanov, and A. D. Stone, *Phys. Rev. E* **62**, 2078 (2000).
- [35] V. A. Podolskiy, E. E. Narimanov, W. Fang, and H. Cao, *Proc. Natl. Acad. Sci. U.S.A.* **101**, 10498 (2004).
- [36] P. Michler *et al.*, *Appl. Phys. Lett.* **77**, 184 (2000).